

Article

Laser Driven Electron Acceleration from Near-Critical Density Targets towards the Generation of High Energy γ -Photons

Iuliana-Mariana Vladisavlevici ^{1,2,*} , Daniel Vizman ³ and Emmanuel d'Humières ¹ ¹ CELIA, University of Bordeaux–CNRS–CEA, 33405 Talence, France² ICAM, West University of Timisoara, 300023 Timisoara, Romania³ Faculty of Physics, West University of Timisoara, 300023 Timisoara, Romania

* Correspondence: iuliana.vladisavlevici@e-uvvt.ro

Abstract: In this paper, we investigate the production of high energy gamma photons at the interaction between an ultra-high intensity laser pulse with an energetic electron beam and with a near-critical density plasma for the laser intensity varying between 10^{19} – 10^{23} W/cm². In the case of the interaction with an electron beam, and for the highest laser intensities considered, the electrons lose almost all their energy to emit gamma photons. In the interaction with a near-critical density plasma, the electrons are first accelerated by the laser pulse up to GeV energies and further emit high energy radiation. A maximum laser-to-photons conversion coefficient of 30% is obtained. These results can be used for the preparation of experiments at the Apollon and ELI laser facilities for the investigation of the emission of high energy γ -photons and to study the electron-positron pair creation in the laboratory.

Keywords: ultra-high intensity regime; near-critical density targets; electron acceleration; high energy photons



Citation: Vladisavlevici, I.-M.; Vizman, D.; d'Humières, E. Laser Driven Electron Acceleration from Near-Critical Density Targets towards the Generation of High Energy γ -Photons. *Photonics* **2022**, *9*, 953. <https://doi.org/10.3390/photonics9120953>

Received: 9 November 2022

Accepted: 6 December 2022

Published: 9 December 2022

Publisher's Note: MDPI stays neutral with regard to jurisdictional claims in published maps and institutional affiliations.



Copyright: © 2022 by the authors. Licensee MDPI, Basel, Switzerland. This article is an open access article distributed under the terms and conditions of the Creative Commons Attribution (CC BY) license (<https://creativecommons.org/licenses/by/4.0/>).

1. Introduction

The generation of intense γ -photon beams from the interaction between an accelerated electron beam and an ultra-high intensity laser is a well-known phenomena [1–3]. Due to the latest advances in laser technology, various theoretical and numerical studies have been performed to optimize the generation of high energy γ -photons using ultra high intensity lasers interacting with matter. At the interaction between an ultra-high intensity laser ($I > 10^{22}$ W/cm²) with a plasma, high energy particle beams can be obtained (protons, electrons, gamma photons, neutrons, etc.). The electrons will be accelerated up to ultra-relativistic velocities and will emit a copious amount of synchrotron gamma photons. Studies on the absorption mechanisms of the laser energy, using different target configurations, showed a conversion efficiency of the laser energy to γ -photons increasing from 0.24% (for a laser intensity of $2 \cdot 10^{21}$ W/cm² [4]) up to 72% (for a laser intensity of 10^{24} W/cm² [5]), as can be observed in Table 1. The highest absorption coefficient of the laser energy to γ -photons are obtained when the laser normalized the field amplitude $a_0 = 0.85(I\lambda^2/10^{18}$ W/cm²)^{1/2} is much higher than the target density normalized by the critical density n_c (where $n_c \approx 1.1 \cdot 10^{21}$ cm⁻³/ $\lambda_{\mu m}^2$ and $\lambda_{\mu m}$ is the laser wavelength in μm). There are multiple applications for these high energy γ -photons for studies involving the creation of electron–positron pairs via the interaction of ultra high energy photons with the laser field, known as the multiphoton Breit-Wheeler process [6,7], the linear Breit-Wheeler process [8,9] and the Bethe-Heitler process [10].

The main goal of this paper is to optimize the emission of high energy γ -photons by high energy electrons accelerated by an ultra-high intensity laser pulse in laser–plasma interaction in the near-critical density regime. To investigate the emission of high energy radiation by the accelerated electrons, we performed multiple 2D Particle-in-cell (PIC) simulations with Simulating Matter Irradiated by Light at Extreme Intensities (SMILEI) [11]

for two cases. In the first case, we analyze the radiation energy losses of an electron beam, which interacts in a head-on collision with an ultra-high intensity laser pulse in a setup similar to the one proposed by M. Vranic et al. [12]. Our goal is to extend the results obtained in [12] to a higher laser intensity (10^{23} W/cm²) and to test the applicability of the multiple radiation reaction models implemented in SMILEI, according to the laser intensity. In the second case, we analyzed the radiation energy losses of the accelerated electrons in the interaction between an ultra-high intensity laser pulse and a near-critical density target. Our objectives are to find the optimum target parameters for the acceleration of the electrons and the emission of high energy radiation, based on a semi-theoretical model of laser energy absorption [13], in the ultra-high intensity near-critical density regime. In both cases, the electrons emit radiation by different mechanisms, according to the interaction regime. In Section 2 the 2D simulation setup for both cases is presented, as well as the mechanisms of radiation energy losses of the electrons along with different models for the effects of the radiation emitted on the electron dynamics implemented in SMILEI [11]. In Section 3, we discuss the results obtained from the 2D PIC simulations. We found a good agreement between the simulations and the theoretical model proposed by M. Vranic et al. [12] for the electron energy losses. Moreover, we found a limit for the classical Landau-Lifshitz model [14] of Radiation Reaction, which depends on the laser intensity. Regarding the laser–plasma interaction, we found an additional dependence of the electron energy losses on the laser pulse duration and target density. Finally, the main results are summarized in Section 4.

Table 1. Conversion coefficient of the laser energy to high energy γ -photons as obtained in theoretical and numerical studies of laser–plasma interaction.

Author	Target	Target Density	Laser Intensity [W/cm ²]	Conversion to γ -Photons Coefficient
Zhang et al. 2022 [4]	cone	exponential from $1n_c$ to $40n_c$	$2 \cdot 10^{21}$	0.24%
Wang et al. 2020 [9]	cylindrical channel	channel: $20n_c$ bulk: $100n_c$	$5 \cdot 10^{22}$	1.5%
Martinez et al. 2020 [15]	C ⁶⁺ plasma	$17n_c$	10^{22}	13%
Brady et al. 2012 [16]	CH ₂ plastic	$100n_c$	$8 \cdot 10^{23}$	15%
Stark et al. 2016 [17]	cylindrical channel	channel: $10n_c$ bulk: $100n_c$	$5 \cdot 10^{22}$	15%
Hadjisolomou et al. 2022 [18]	Lithium foil	$102n_c$	10^{23}	30%
Ridgers et al. 2012 [7]	Aluminium foil	$780n_c$	$8 \cdot 10^{23}$	35%
Lobet et al. 2015 [19]	Aluminium foil	$780n_c$	$8.9 \cdot 10^{23}$	65%
Ji et al. 2014 [5]	Hydrogen plasma	$32n_c$	10^{24}	72%

2. High Energy Radiation Emitted by the Energetic Electrons

2.1. Laser-Electron Beam Interaction

The 2D PIC simulation setup for the first case scenario is shown in Figure 1: an ultra-high intensity laser pulse interacting with an energetic electron beam. The linearly polarized laser pulse has the following parameters: a variable laser pulse intensity in the range 10^{19} – 10^{23} W/cm², a pulse duration of 30 fs FWHM, a wavelength 1 μ m and a focal spot size of $w_0 = 3 \mu$ m. The laser is focused at the middle of the simulation box. The

electron beam characteristics are: electron density $10^{-5}n_c$, longitudinal width $L_x = 0.8 \mu\text{m}$ and transversal width $L_y = 0.16 \mu\text{m}$. The initial electron beam energy varies in $\{0.5, 1, 1.5\}$ GeV. The simulation box has $30 \mu\text{m}$ in the x direction, and $4 \mu\text{m}$ in the y direction. The cell length is $dx = dy = 15.625 \text{ nm}$ and the number of particles per cell is 32. The particles are deleted while crossing the domain boundaries and the fields are absorbed. A total number of 18 PIC simulations were performed with SMILEI [11].

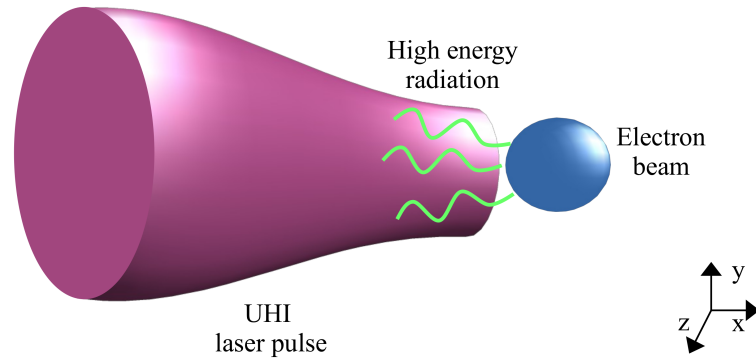


Figure 1. An ultra high intensity laser pulse colliding with an energetic electron beam. The laser parameters are: wavelength $\lambda = 1 \mu\text{m}$, peak intensity $I : \{10^{19}\text{--}10^{23}\} \text{ W/cm}^2$, pulse duration $\tau = 30 \text{ fs}$ FWHM and focal spot size $w_0 = 3 \mu\text{m}$. For the 2D simulation setup, the electron beam parameters are: $n_{e0} = 10^{-5}n_c$, $L_x = 0.8 \mu\text{m}$, $L_y = 0.16 \mu\text{m}$ and $\epsilon_{e0} : \{0.5, 1, 1.5\} \text{ GeV}$.

At the interaction with the laser pulse, the electrons are losing energy by emitting high energy radiation mainly along the direction of their own motion, with a small range of angles around the direction of its velocity:

$$\theta \sim \sqrt{1 - \frac{v^2}{c^2}} \tag{1}$$

The electron energy loss is given by [12]:

$$\frac{\Delta\epsilon}{\epsilon_{e0}} = - \frac{k\gamma_i^2}{(\gamma_i - 1)(1 + k\gamma_i)} \tag{2}$$

where $\Delta\epsilon$ represents the difference between the initial and final electron energy, ϵ_{e0} —the initial electron energy, γ_i —the initial relativistic Lorentz factor of the electron and:

$$k = 3.2 \times 10^{-5} I_0 \left[\frac{10^{22} \text{W}}{\text{cm}^2} \right] \tau [\text{fs}] (1 - \cos \theta)^2$$

with I_0 —the laser pulse intensity, τ —the pulse duration and θ —the angle of interaction between the laser and the electron beam.

The radiation emitted can influence the dynamics of the particle. This phenomena is known as the radiation reaction. There are different regimes for the emission of radiation and its effect on the particle dynamics implemented in SMILEI [20]. They are characterized by the particle quantum parameter [11]:

$$\chi = \frac{\gamma}{E_s} \sqrt{(\vec{E} + \vec{v} \times \vec{B})^2 - \frac{(\vec{v} \cdot \vec{E})^2}{c^2}} \tag{3}$$

where $\gamma = \epsilon/m_e c^2$ is the particle Lorentz factor, \vec{v} is the particle velocity, \vec{E}, \vec{B} —the electric, respectively; the magnetic field of the laser and E_s is the Schwinger field given by:

$$E_s = \frac{m_e^2 c^3}{e\hbar} = 1.3 \times 10^{16} \text{ V/cm} \tag{4}$$

The Schwinger field is used as a reference for nonlinear quantum electrodynamics effects such as pair production in the vacuum. This field corresponds to an intensity of $I = 10^{29}$ W/cm², which is far from what we can achieve in the present laser facilities. However, in [21], it was demonstrated that the intensity is much higher in the rest frame of the relativistic electrons, in such a way that radiation reaction effects can be studied experimentally at laser facilities such as Apollon [22] and ELI [23].

For a parameter $\chi \ll 1$, the radiation reaction is described through the classical model proposed by Landau Lifshitz (for $\chi \sim 10^{-3}$) and a corrected Landau-Lifshitz model (for $\chi \sim 10^{-2}$). In this case, the electrons lose continuous energy by radiation and the radiation will act on the electron dynamics like a damping force [14]. The energy of the emitted photons is much smaller than the energy of the emitting electrons.

When the χ parameter approaches 1, the continuous models cannot be used anymore, the emission of photons being better described as a stochastic event. In the case of a weak quantum regime $\chi \sim 10^{-1}$, the description is made by the Niel model [24], where to the Landau-Lifshitz damping forces is added a term linked to the stochasticity of the emission of photons. In this case, the energy of the photons remains small with respect to that of the emitting electrons. When $\chi \sim 1$, the emitted photon energies are of the order of the emitting electron energies. In this case, the emission of photons is described only by a stochastic Monte Carlos process, which is computed as a function of the particle field and energy [11].

2.2. Laser–Plasma Interaction

For the second case scenario considered, of an ultra-high intensity laser pulse interacting with a near-critical density plasma, the emission of high energy radiation will take place in two steps: the acceleration of the electrons by the laser pulse and the emission of radiation by the accelerated electrons.

For the PIC simulation setup, we considered a similar setup as the one from Figure 1, where instead of the electron beam we have a near-critical density plasma. The laser is linearly polarized and has the following characteristics: a wavelength of 1 μm , a focal spot size of 4π μm , a pulse duration of 20 fs FWHM ($6t_0$) for the laser intensity varying in 10^{20} – 10^{23} W/cm² (corresponding to a normalized field amplitude of $a_0 = 8.5$ – 268.8) and a laser intensity of 10^{22} W/cm² for the pulse duration varying in 6.5–100 fs FWHM ($2t_0$ – $30t_0$). The laser is focused at the middle of the simulation box. The target is considered fully ionized, being made of protons and electrons. The density of the target varies from $0.5n_c$ to $20n_c$ (where $n_c \approx 1.1 \cdot 10^{21}$ cm⁻³ is the critical density for a wavelength of 1 micron), while the thickness varies from 500 nm to 200 μm . The transversal width of the target is kept constant at 30 μm . The simulation box has 60 μm in the y direction, while in the x direction it is changed according to the thickness L_x of the target from 120 μm to 300 μm . The cell length is $dx = dy = 15.625$ nm and the number of particles per cell is 30 for each species. The particles are deleted while crossing the domain boundaries and the fields are absorbed. A total number of 116 PIC simulations were performed with SMILEI [11] on the Curta machine—MCIA supercomputer [25].

3. Results and Discussion

3.1. High Energy Radiation in Laser–Electron Beam Interaction

The results obtained from 2D PIC simulations and from Equation (2) are given in Figure 2. The energy loss becomes significant for laser intensities higher than 10^{20} W/cm². For the highest intensity considered, 10^{23} W/cm², the electrons are losing almost all their energy in the emission of γ -photons. The electron beam energy also plays a role: the more energetic the electrons are, the more important is the emission of radiation.

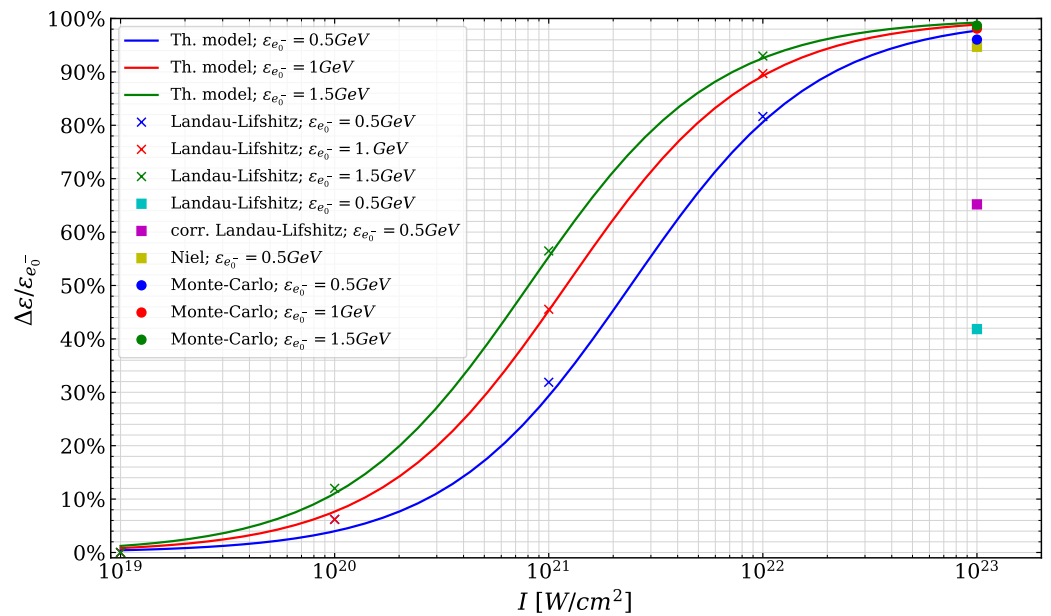


Figure 2. Electron energy loss vs. laser intensity as obtained from 2D PIC simulations. The continuous lines (blue— $\epsilon_{e_0^-} = 0.5 \text{ GeV}$, red— $\epsilon_{e_0^-} = 1 \text{ GeV}$, green— $\epsilon_{e_0^-} = 1.5 \text{ GeV}$) represent the theoretical scaling from Equation (2). The simulation results are represented as follows: the continuous Landau-Lifshitz model—crosses (blue— $\epsilon_{e_0^-} = 0.5 \text{ GeV}$, red— $\epsilon_{e_0^-} = 1 \text{ GeV}$, green— $\epsilon_{e_0^-} = 1.5 \text{ GeV}$); for $I = 10^{23} \text{ W/cm}^2$: continuous Landau-Lifshitz model—azure square, corrected Landau-Lifshitz model—magenta square, stochastic Niel model—yellow square and stochastic Monte Carlo model—circles (blue— $\epsilon_{e_0^-} = 0.5 \text{ GeV}$, red— $\epsilon_{e_0^-} = 1 \text{ GeV}$, green— $\epsilon_{e_0^-} = 1.5 \text{ GeV}$).

The classical Landau-Lifshitz model used in our simulations fits the predicted theoretical results of Equation (2) up to the laser intensity of 10^{22} W/cm^2 . Above this intensity, the classical model and the corrected continuous model underestimate the radiation emitted by the electrons. For ultra-high intensities, the electrons lose a significant part of their energy, and the phenomena cannot be anymore assumed to involve continuous energy transfers. To compute the transfer of energy from the electrons to the photons, stochastic models must be used. The best approximation of the theoretical results is given by the Monte Carlo model.

Figure 3 shows the energy angle distribution of the emitted radiation by an energetic electron beam of initial energy $\epsilon_{e_0^-} = 1.5 \text{ GeV}$ at the interaction with a high intensity laser pulse for two intensities: 10^{22} W/cm^2 and 10^{23} W/cm^2 . The laser propagation direction is at $\theta = 0^\circ$, while the electrons are counterpropagating at $\theta = 180^\circ$. The high-energy radiation is emitted mostly in the direction of the moving electrons or at small angles around their direction, as theoretically predicted by Equation (1). Moreover, the emission of radiation significantly increases in the case of $I = 10^{23} \text{ W/cm}^2$ in multiple directions, with the preferential direction around $\theta = 180^\circ$.

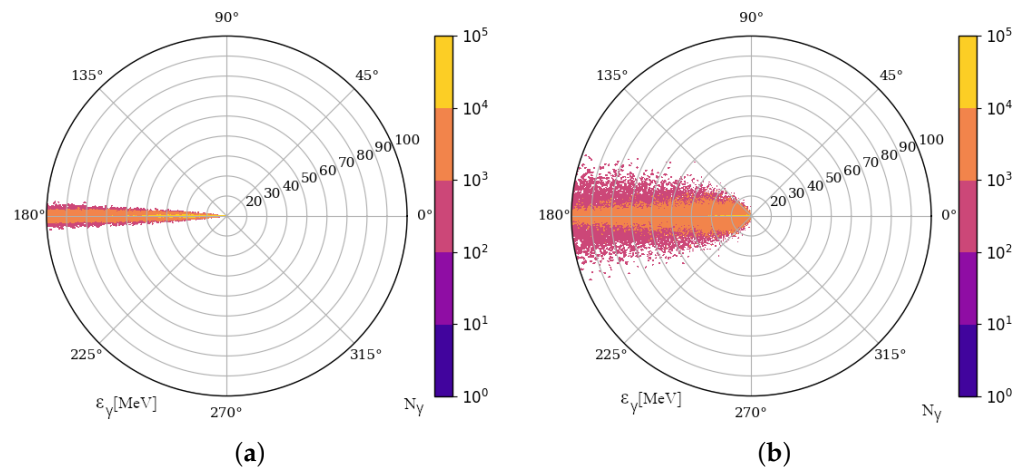


Figure 3. The energy angle distributions of the emitted radiation with the energy up to 100 MeV at 185 fs, integrated in time, for different laser intensities: (a) $I = 10^{22}$ W/cm² (b) $I = 10^{23}$ W/cm². Laser parameters: $\lambda = 1 \mu\text{m}$, $\tau = 30\text{fs}$ FWHM and $w_0 = 3 \mu\text{m}$. Electron beam parameters: $n_{e0} = 10^{-5}n_c$, $L_x = 0.8 \mu\text{m}$, $L_y = 0.16 \mu\text{m}$ and $\varepsilon_{e_0} = 1.5 \text{ GeV}$. The cutoff energy of the energy angle distribution is: (a) 1150 MeV and (b) 1200 MeV.

3.2. Laser-Driven Electron Acceleration in the Laser–Plasma Interaction Case

In the laser–plasma interaction case, at the interaction of the laser pulse with the target, the electrons (being lighter than the protons) will be accelerated by the laser ponderomotive force $f_p = -m_e c^2 \gamma_a$, where $\gamma_a = (1 + a_0^2/2)^{1/2}$ and a_0 is the laser-normalized field amplitude. The electrons are pushed forward by the laser field much faster than the protons. The later ones, having a small charge-to-mass ratio, will be left behind. This charge displacement occurring inside the target will create a very strong quasi-static charge separation field at the back of the target. The faster electrons will escape the potential created at the back of the target; meanwhile, the slower ones will be reinjected in the target, forming a counterpropagating current. In Figure 4, the absorption coefficient of the laser energy to electrons vs. target areal density is shown. The dependence of the absorption coefficient of the laser energy to electrons is very similar to the total absorption coefficient dependence on the target areal density from [13]: the absorption coefficient of the laser energy to electrons increases when the target thickness increases, eventually reaching a plateau, and additional plasma into the target will not affect it significantly.

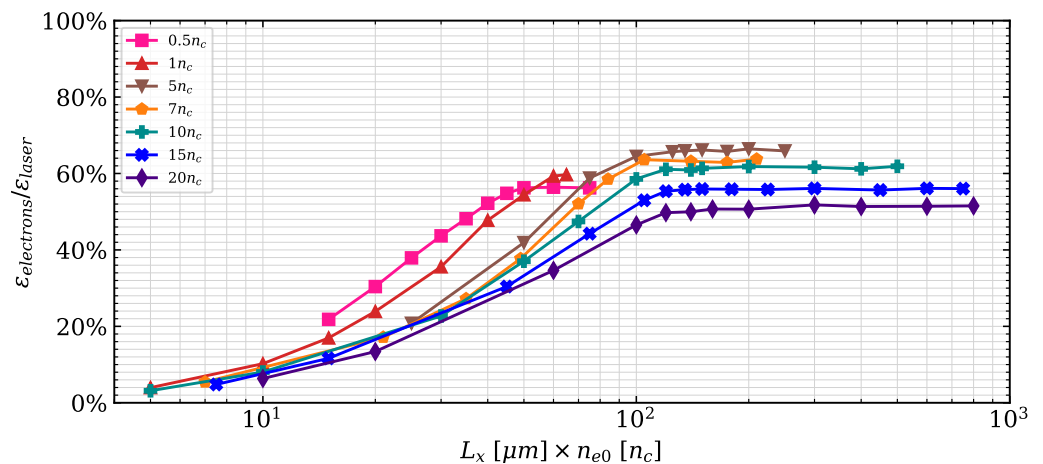


Figure 4. Energy conversion coefficient from the laser to electrons vs. target areal density as obtained in 2D PIC simulations. Target parameters: $L_y = 30 \mu\text{m}$. Laser parameters: $\lambda = 1 \mu\text{m}$, $a_0 = 85$, $\tau = 20 \text{ fs}$ FWHM and $w_0 = 12.5 \mu\text{m}$.

The electrons present a broad spectrum, as shown in Figure 5 with two main populations: a less energetic one, with the energy between 5 MeV and 400 MeV, and a high energy one, with the energy higher than 400 MeV. The lower energy population represents the electrons, which recirculate inside the target and will help to the further acceleration of the ions by sustaining the electrostatic field at the back of the target [26,27]. The high energy population represents the electrons, which escape the electrostatic potential and travel free in the vacuum behind the target.

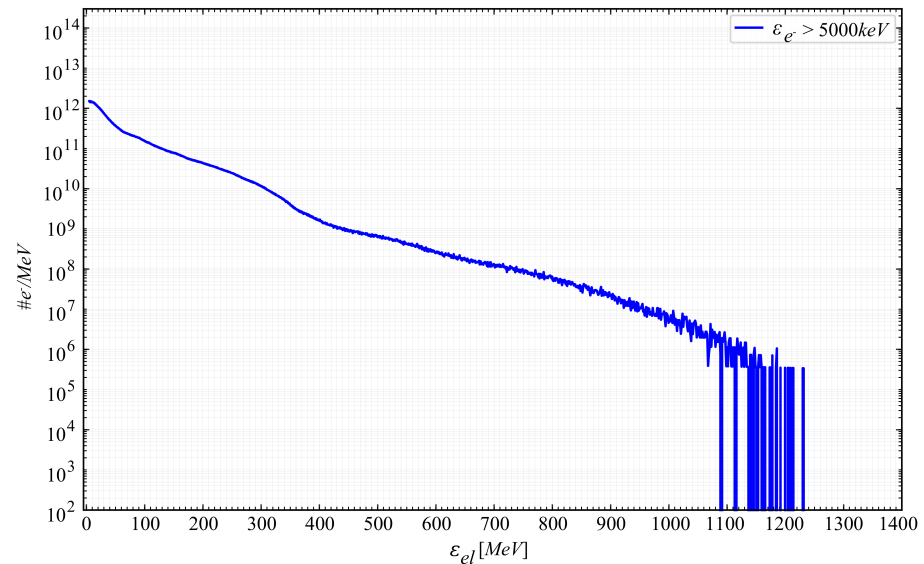


Figure 5. Electron spectra from a 2D PIC simulation. Target parameters: $n_{e0} = 3n_c$, $L_x = 40 \mu\text{m}$ and $L_y = 30 \mu\text{m}$. Laser parameters: $\lambda = 1 \mu\text{m}$, $a_0 = 85$, $\tau = 20 \text{ fs FWHM}$ and $w_0 = 12.5 \mu\text{m}$.

The acceleration of electrons is made at ultra-relativistic level, their maximum energy being in the range of hundreds of MeV – GeV, as shown in Figure 6. The evolution of the maximum energy of the electrons as a function of the target areal density shows an optimum point, which is reached before the saturation point of the laser-to-electrons energy conversion coefficient. For a thicker and denser target than the optimum values for acceleration, the electrons will be heated in a larger volume, which will lead to a lower electron energy density.

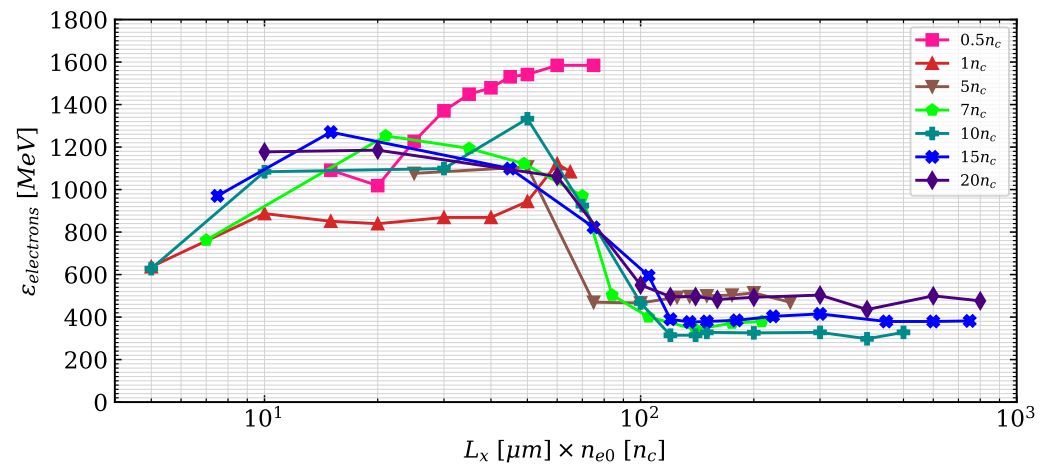


Figure 6. Maximum electron energy vs target areal density, as obtained in 2D PIC simulations. Target parameters: $L_y = 30 \mu\text{m}$. Laser parameters: $\lambda = 1 \mu\text{m}$, $a_0 = 85$, $\tau = 20 \text{ fs FWHM}$ and $w_0 = 12.5 \mu\text{m}$.

The maximum energy of the electrons depends also on the laser parameters. To study this effect, we varied the laser pulse intensity for a fixed pulse duration and, respectively, we varied the laser pulse duration for a fixed laser intensity. The target density was varying between $0.5n_c$ and $20n_c$ and for each target density, we considered the optimum thickness to maximize the transfer of energy from the laser pulse to the plasma, as explained in [13], which is between 0.5–200 μm . The target width was kept constant at 30 μm , as in the previous case.

For a fixed laser pulse duration of $6t_0$, we varied the laser intensity in the range of 10^{20} – 10^{23} W/cm^2 , corresponding to a normalized field amplitude of 8.5–268.8. In Figure 7, the variation of the maximum electron energy is shown with the target density for various laser intensities.

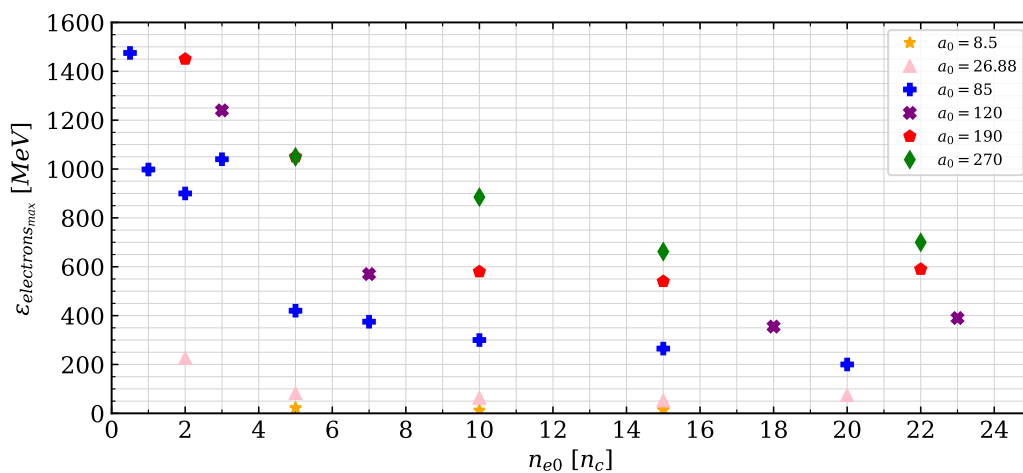


Figure 7. Maximum electron energy at the optimum target thickness vs. target density for various laser pulse intensities. Target parameters: $L_y = 30 \mu\text{m}$. Laser parameters: $\lambda = 1 \mu\text{m}$, $\tau = 6t_0$ and $w_0 = 12.5 \mu\text{m}$.

The maximum electron energy varies from a few tens of MeV for low laser intensities up to >1 GeV for ultra-high laser intensities. In addition, for the same intensity, we have a strong variation of the maximum energy: from 200 MeV to 1.5 GeV for $a_0 = 85$. This is due to the dependence of the maximum electron energy on the target density. The maximum energies are obtained for the lowest target density. For targets with densities $> 10n_c$, the maximum electron energy varies slowly in the range considered for the same laser pulse intensity.

For a fixed $a_0 = 85$, we varied the pulse duration in the range 2–30 t_0 . In Figure 8 the variation of the maximum electron energy is shown with the target density for various laser pulse durations.

The maximum electron energy varies from a few hundreds of MeV up to 1.5 GeV. In addition, the previously explained behaviour is present: for the same pulse duration, the maximum electron energy varies dramatically due to the target density. The highest electron energy is obtained for the longest pulse duration, corresponding to the highest laser energy used in this variation, and the lowest target density considered. For targets with densities $> 10n_c$, the maximum electron energy varies slowly in the range considered for the same laser pulse duration.

In the ultra-relativistic regime, the energetic electrons will be subject to Inverse Compton Scattering, emitting radiation at the interaction with the high intensity laser field. The emission of the radiation will be mainly in the direction of the electron propagation.

In the following section, we will describe the emission of radiation in the transparent and opaque regimes.

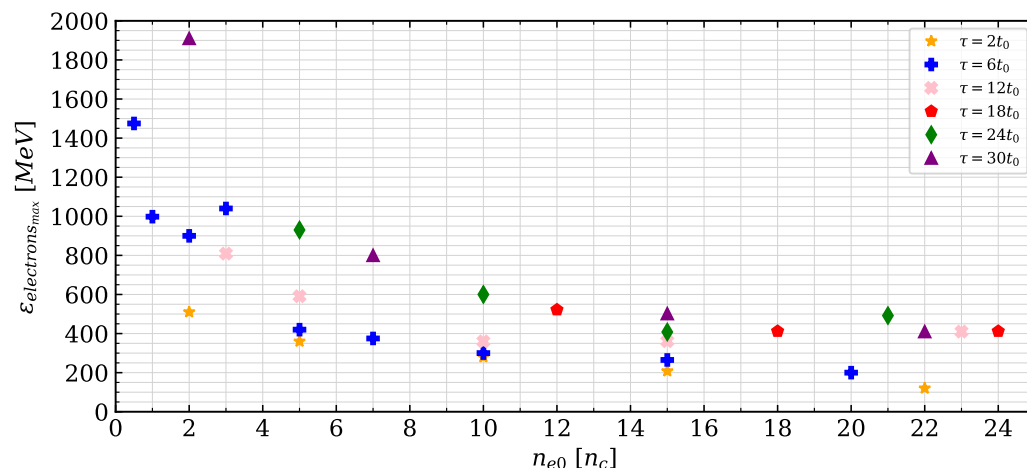


Figure 8. Maximum electron energy at the optimum target thickness vs target density for various laser pulse durations. Target parameters: $L_y = 30 \mu\text{m}$. Laser parameters: $\lambda = 1 \mu\text{m}$, $a_0 = 85$ and $w_0 = 12.5 \mu\text{m}$.

3.3. Emission of High Energy Radiation in Laser–Plasma Interaction

According to the target density, we can identify two regimes of the emission of high energy radiation in the laser–plasma interaction: Reinjecting Electron Synchrotron Emission [7] and Skin-depth emission [16].

In the case of an underdense target of the $0.1n_c$ density, interacting with a laser pulse of intensity $I = 10^{22} \text{ W/cm}^2$, the laser ponderomotive force will push the electrons in the forward direction, accelerating them up to relativistic velocities. The ions will respond slower to the laser force, while the hot electrons will be escaping the target in the forward direction. This separation of charges inside the target will set up a strong longitudinal electric field at the back of the target. This charge–separation field will in turn recirculate inside some of the electrons and accelerate the ions. At the interaction of the backward accelerated electrons with the laser pulse, they will suffer a strong synchrotron emission of γ -photons in their direction of propagation. Figure 9 (left) shows the angular distribution of the emitted γ -ray energy. As the laser continuously pushes forward electrons, the charge–separation field will reinject them again, and another emission of radiation will occur. The process will repeat itself with a periodicity called ‘break-down time’, proportional to the laser period. This process is known as Reinjecting Electron Synchrotron Emission (RESE) and it can convert up to 15% of the laser energy into γ -photons [7].

In the case of an overdense target of $20n_c$ density, interacting with a laser pulse of intensity $I = 10^{22} \text{ W/cm}^2$, the laser pressure will create a hole-boring front over the target surface, from which a part of the laser beam will be reflected. The reflected wave will interact with the forward accelerated electrons and will give rise to an emission of radiation predominantly in the forward direction, as shown in Figure 9b. This process is known as skin-depth emission and is specific to relativistic overdense targets [16].

As previously mentioned, the relativistic electrons will emit a copious amount of high energy radiation. In Figure 10, the variation of the absorption coefficient of the laser energy to high energy photons is shown with the target density for various laser pulse intensities. The absorption coefficient in high energy photons increases from $\leq 1\%$ for a laser intensity of $I = 10^{20} \text{ W/cm}^2$ ($a_0 = 8.5$) to 30% for ultra-high intensity laser pulses $I = 10^{23} \text{ W/cm}^2$ ($a_0 = 268.8$). For laser intensities $> 10^{22} \text{ W/cm}^2$, for the same intensity, the absorption into high energy photons does not vary significantly with the target density in the range considered.

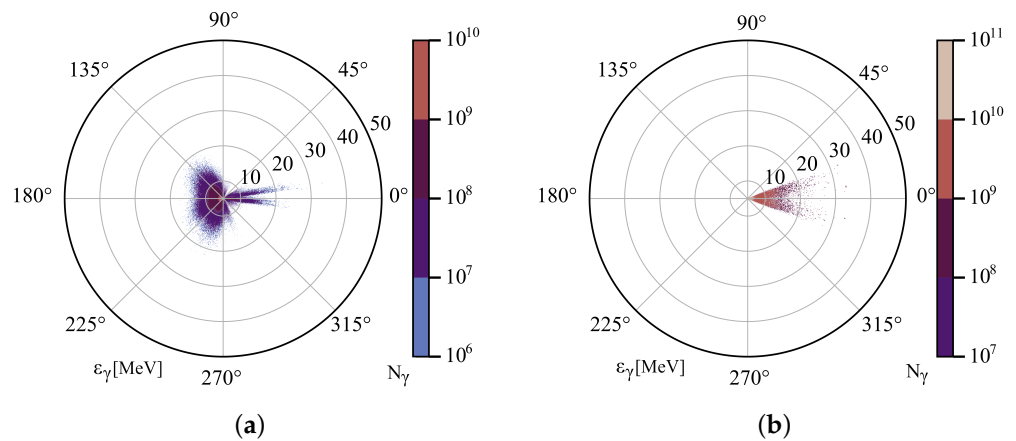


Figure 9. The energy angle distribution of the emitted γ -photons integrated in time, at 300 fs after the laser–plasma interaction begins, as obtained from a 2D PIC simulation. Laser parameters: $\lambda = 1 \mu\text{m}$, $a_0 = 85$, $\tau = 20$ fs FWHM and $w_0 = 12.5 \mu\text{m}$. (a) Target parameters: $n_{e0} = 0.1n_c$, $L_x = 120 \mu\text{m}$ and $L_y = 30 \mu\text{m}$. (b) Target parameters: $n_{e0} = 20n_c$, $L_x = 50 \mu\text{m}$ and $L_y = 30 \mu\text{m}$.

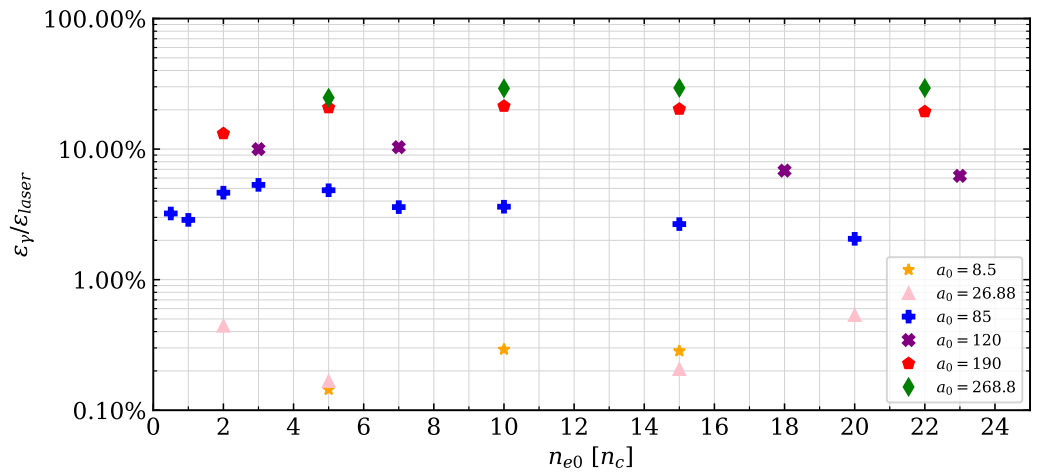


Figure 10. Absorption coefficient from the laser pulse to high energy photons at the optimum target thickness vs. target density for different laser intensities. Target parameters: $L_y = 30 \mu\text{m}$. Laser parameters: $\lambda = 1 \mu\text{m}$, $\tau = 20$ fs FWHM and $w_0 = 12.5 \mu\text{m}$.

In Figure 11 the variation of the absorption coefficient of the laser energy to high energy photons is shown with the target density for various laser pulse durations for $a_0 = 85$. The absorption coefficient in high energy photons increases from $\leq 1\%$ for a very short pulse duration ($\tau = 2t_0$) to 10% for longer pulse duration ($\tau = 30t_0$). For laser pulse durations longer than 20 fs, for the same pulse duration, the absorption into high energy photons does not vary significantly with the target density in the range considered.

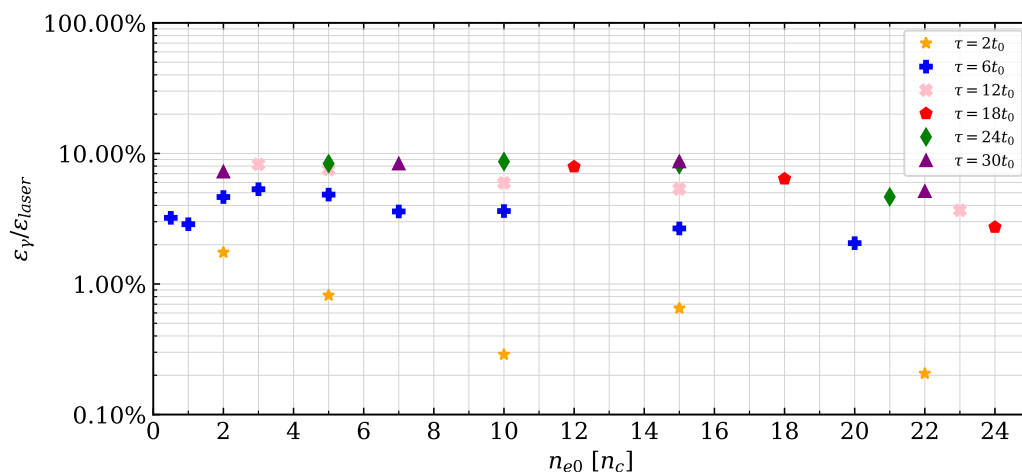


Figure 11. Absorption coefficient from the laser pulse to high energy photons at the optimum target thickness vs. target density for different laser pulse durations. Target parameters: $L_y = 30 \mu\text{m}$. Laser parameters: $\lambda = 1 \mu\text{m}$, $a_0 = 85$ and $w_0 = 12.5 \mu\text{m}$.

4. Conclusions

We studied the high-energy radiation produced in two configurations: laser–electron beam interaction and laser–plasma interaction. Varying the intensity of the laser pulse in $\{10^{19} : 10^{23}\} \text{ W/cm}^2$, we studied the production of gamma photons for different initial energies of the electron beam (0.5, 1, 1.5 GeV) extending the results obtained by M. Vranic et al. [12]. For the highest laser intensity, we considered the electrons losing almost all of their energy to emit γ -photons. In addition, we compared different models implemented in SMILEI for the emission of radiation and its effect on the electron dynamics. We found that for the highest laser intensity considered, the continuous Landau-Lifshitz models cannot be used anymore and a stochastic model should be used instead. In the second configuration, we considered a laser pulse of intensity varying in 10^{20} – 10^{23} W/cm^2 for a pulse duration of 20 fs FWHM, and the pulse duration varying in 6.5–100 fs for a laser intensity of 10^{22} W/cm^2 irradiating a near-critical density target with the density in 0.5 – $20n_c$ and thickness in 0.5 – $200 \mu\text{m}$. The maximum absorption coefficient in gamma photons for various laser intensities was 30% for the highest laser intensity considered. The photons will have energies similar to the ones of the electrons which emitted them, corresponding to hundreds of MeV–GeV. This opens up the possibility to study new regimes of laser–plasma interactions in extreme conditions at Apollon and ELI laser facilities. Our results can be used in experiments at these facilities, involving electron acceleration to high energies and the emission of high energy radiation in the ultra-high intensity near-critical density regime towards electron–positron pair creation via the interaction of high energy photons with the laser field, known as the nonlinear or multiphoton Breit-Wheeler process [6,28].

Author Contributions: Conceptualization, I.-M.V. and E.d.; methodology, I.-M.V., E.d., and D.V.; software, I.-M.V.; validation, I.-M.V. and E.d.; formal analysis, I.-M.V.; investigation, I.-M.V. and E.d.; resources, E.d. and D.V.; data curation, I.-M.V.; writing—original draft preparation, I.-M.V.; writing—review and editing, I.-M.V., E.d., and D.V.; visualization, I.-M.V., E.d., and D.V.; supervision, E.d. and D.V.; project administration, E.d. and D.V.; funding acquisition, E.d. and D.V. All authors have read and agreed to the published version of the manuscript.

Funding: This work was supported by the Romanian National Authority for Scientific Research PN 75/2018, Agence Nationale de la Recherche project ANR-17-CE30-0026-Pinnacle, WUT-JINR collaboration project 05-6-1119-2014/2023 (2/2019; 86/2020; 103/2021) and Erasmus+ Student grant (2018/2019; 2019/2020; 2020/2021). The authors acknowledge support by GENCI, France for awarding us access to HPC resources at TGCC/CCRT (Grant No. A0110512943).

Data Availability Statement: The data that support the findings of this study are available from the corresponding author upon reasonable request.

Acknowledgments: The computer time for this study was provided by the computing facilities MCIA (Mésocentre de Calcul Intensif Aquitain) of the Université de Bordeaux and of the Université de Pau et des Pays de l'Adour [25]. We acknowledge the technical support of the SMILEI team.

Conflicts of Interest: The authors declare no conflict of interest.

References

1. Wang, H.Y.; Yan, X.Q.; Zepf, M. Signatures of quantum radiation reaction in laser-electron-beam collisions. *Phys. Plasmas* **2015**, *22*, 093103. [CrossRef]
2. Vranic, M.; Grismayer, T.; Fonseca, R.A.; Silva, L.O. Quantum radiation reaction in head-on laser-electron beam interaction. *New J. Phys.* **2016**, *18*, 073035. [CrossRef]
3. Bulanov, S.V.; Esirkepov, T.Z.; Hayashi, Y.; Kando, M.; Kiriya, H.; Koga, J.K.; Kondo, K.; Kotaki, H.; Pirozhkov, A.S.; Bulanov, S.S.; et al. On the design of experiments for the study of extreme field limits in the interaction of laser with ultrarelativistic electron beam. *Nucl. Instruments Methods Phys. Res. A* **2011**, *660*, 31–42. [CrossRef]
4. Zhang, C.-W.; Zhu, Y.-X.; Lv, J.-F.; Xie, B.-S. Simulation Study of a Bright Attosecond γ -ray Source Generation by Irradiating an Intense Laser on a Cone Target. *Appl. Sci.* **2022**, *12*, 4361. [CrossRef]
5. Ji, L.L.; Pukhov, A.; Nerush, E.N.; Kostyukov, I.Y.; Shen, B.F.; Akli, K.U. Energy partition, γ -ray emission, and radiation reaction in the near-quantum electrodynamic regime of laser-plasma interaction. *Phys. Plasmas* **2014**, *21*, 023109. [CrossRef]
6. Breit, G.; Wheeler, J.A. Collision of Two Light Quanta. *Phys. Rev.* **1934**, *46*, 1087–1091. [CrossRef]
7. Ridgers, C.P.; Brady, C.S.; Ducloux, R.; Kirk, J.G.; Bennett, K.; Arber, T.D.; Robinson, A.P.L.; Bell, A.R. Dense Electron-Positron Plasmas and Ultraintense γ rays from Laser-Irradiated Solids. *Phys. Rev. Lett.* **2012**, *108*, 165006. [CrossRef] [PubMed]
8. Ribeyre, X.; d'Humières, E.; Jansen, O.; Jequier, S.; Tikhonchuk, V.T.; Lobet, M. Pair creation in collision of γ -ray beams produced with high-intensity lasers. *Phys. Rev. E* **2016**, *93*, 013201. [CrossRef]
9. Wang, T.; Ribeyre, X.; Gong, Z.; Jansen, O.; d'Humières, E.; Stutman, D.; Toncian, T.; Arefiev, A. Power Scaling for Collimated γ -Ray Beams Generated by Structured Laser-Irradiated Targets and Its Application to Two-Photon Pair Production. *Phys. Rev. Appl.* **2020**, *13*, 054024. [CrossRef]
10. Chen, H.; Wilks, S.C.; Bonlie, J.D.; Liang, E.P.; Myatt, J.; Price, D.F.; Meyerhofer, D.D.; Beiersdorfer, P. Relativistic Positron Creation Using Ultraintense Short Pulse Lasers. *Phys. Rev. Lett.* **2009**, *102*, 105001. [CrossRef]
11. Derouillat, J.; Beck, A.; Pérez, F.; Vinci, T.; Chiaramello, M.; Grassi, A.; Flé, M.; Bouchard, G.; Plotnikov, I.; Aunai, N.; et al. SMILEI: A collaborative, open-source, multi-purpose particle-in-cell code for plasma simulation. *Comput. Phys. Commun.* **2018**, *222*, 351–373. [CrossRef]
12. Vranic, M.; Martins, J.L.; Vieira, J.; Fonseca, R.A.; Silva, L.O. All-Optical Radiation Reaction at 10^{21} W/cm². *Phys. Rev. Lett.* **2014**, *113*, 134801. [CrossRef] [PubMed]
13. Vladisavljević, I.M.; Vizman, D.; Humières, E.D. Theoretical investigation of the interaction of ultra-high intensity laser pulses with near critical density plasmas. *In preparation*.
14. Landau, L.D.; Lifshitz, E.M. *The Classical Theory of Fields*, 3rd ed.; Pergamon Press: Oxford, UK, 1971.
15. Martinez, B.; d'Humières, E.; Gremillet, L. Synchrotron radiation from ultrahigh-intensity laser-plasma interactions and competition with Bremsstrahlung in thin foil targets. *Phys. Rev. Res.* **2020**, *2*, 043341. [CrossRef]
16. Brady, C.S.; Ridgers, C.P.; Arber, T.D.; Bell, A.R.; Kirk, J.G. Laser Absorption in Relativistically Underdense Plasmas by Synchrotron Radiation. *Phys. Rev. Lett.* **2012**, *109*, 245006. [CrossRef]
17. Stark, D.J.; Toncian, T.; Arefiev, A.V. Enhanced Multi-MeV Photon Emission by a Laser-Driven Electron Beam in a Self-Generated Magnetic Field. *Phys. Rev. Lett.* **2016**, *116*, 185003. [CrossRef]
18. Hadjisolomou, P.; Jeong, T.M.; Bulanov, S.V. Towards bright gamma-ray flash generation from tailored target irradiated by multi-petawatt laser. *Sci. Rep.* **2022**, *12*, 17143. [CrossRef]
19. Lobet, M.; Ruyer, C.; Debayle, A.; d'Humières, E.; Grech, M.; Lemoine, M.; Gremillet, L. Ultrafast Synchrotron-Enhanced Thermalization of Laser-Driven Colliding Pair Plasmas. *Phys. Rev. Lett.* **2015**, *115*, 215003. [CrossRef]
20. Lobet, M.; d'Humières, E.; Grech, M.; Ruyer, C.; Davoine, X.; Gremillet, L. Modeling of radiative and quantum electrodynamics effects in PIC simulations of ultra-relativistic laser-plasma interaction. *J. Phys. Conf. Ser.* **2016**, *688*, 012058. [CrossRef]
21. Di Piazza, A.; Hatsagortsyan, K.Z.; Keitel, C.H. Quantum Radiation Reaction Effects in Multiphoton Compton Scattering. *Phys. Rev. Lett.* **2010**, *105*, 220403. [CrossRef]
22. Centre Interdisciplinaire Lumière Extrême. Available online: <https://cilexsaclay.fr> (accessed on 8 December 2022).
23. Extreme Light Infrastructure. Available online: <https://eli-laser.eu/> (accessed on 8 December 2022).
24. Niel, F.; Riconda, C.; Amiranoff, F.; Ducloux, R.; Grech, M. From quantum to classical modelling of radiation reaction: A focus on stochasticity effects. *Phys. Rev. E* **2018**, *97*, 043209. [CrossRef] [PubMed]
25. Mésocentre de Calcul Intensif Aquitain. Available online: <https://redmine.mcia.fr/projects/cluster-curta/> (accessed on 2 September 2022).
26. Snavely, R.A.; Key, M.H.; Hatchett, S.P.; Cowan, T.E.; Roth, M.; Phillips, T.W.; Stoyer, M.A.; Henry, E.A.; Sangster, T.C.; Singh, M.S.; et al. Intense High-Energy Proton Beams from Petawatt-Laser Irradiation of Solids. *Phys. Rev. Lett.* **2000**, *85*, 2945. [CrossRef] [PubMed]

-
27. Wilks, S.C.; Langdon, A.B.; Cowan, T.E.; Roth, M.; Singh, M.; Hatchett, S.; Key, M.H.; Pennington, D.; MacKinnon, A.; Snavely, R.A. Energetic proton generation in ultra-intense laser–solid interactions. *Phys. Plasma* **2001**, *8*, 542–549. [[CrossRef](#)]
 28. Burke, D.L.; Field, R.C.; Horton-Smith, G.; Spencer, J.E.; Walz, D.; Berridge, S.C.; Bugg, W.M.; Shmakov, K.; Weidemann, A.W.; Bula, C.; et al. Positron Production in Multiphoton Light-by-Light Scattering. *Phys. Rev. Lett.* **1997**, *79*, 1626–1629. [[CrossRef](#)]